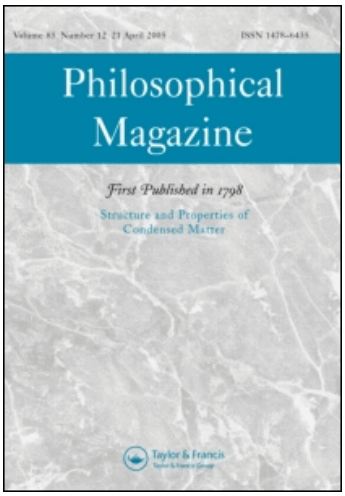

Philosophical Magazine
Publication details, including instructions for authors and subscription information:
http://www.informaworld.com/smpp/title~content=t713695589

Energy dissipation in fracture of bulk metallic glasses via inherent competition between local softening and quasi-cleavage

M. Q. Jiang [a]; Z. Ling [a]; J. X. Meng [a]; L. H. Dai
[a] State Kay Laboratory of Nonlinear Mechanics, Institute of Mechanics, Chinese Academy of Science, Beijing 100080, China

Online Publication Date: 01 January 2008

To cite this Article Jiang, M. Q., Ling, Z., Meng, J. X. and Dai, L. H.(2008)'Energy dissipation in fracture of bulk metallic glasses via inherent competition between local softening and quasi-cleavage',Philosophical Magazine,88:3,407 — 426

To link to this Article: DOI: 10.1080/14786430701864753

URL: http://dx.doi.org/10.1080/14786430701864753

Philosophical Magazine,
Vol. 88, No. 3, 21 January 2008, 407–426

Taylor & Francis
Taylor & Francis Group

Energy dissipation in fracture of bulk metallic glasses via inherent competition between local softening and quasi-cleavage

M. Q. JIANG, Z. LING, J. X. MENG and L. H. DAI*

State Kay Laboratory of Nonlinear Mechanics, Institute of Mechanics, Chinese Academy of Science, Beijing 100080, China

(*Received 25 November 2007; in final form 10 December 2007*)

Compression, tension and high-velocity plate impact experiments were performed on a typical tough $Zr_{41.2}Ti_{13.8}Cu_{10}Ni_{12.5}Be_{22.5}$ (Vit 1) bulk metallic glass (BMG) over a wide range of strain rates from $\sim 10^{-4}$ to $10^{6}\,s^{-1}$. Surprisingly, fine dimples and periodic corrugations on a nanoscale were also observed on dynamic mode I fracture surfaces of this tough Vit 1. Taking a broad overview of the fracture patterning of specimens, we proposed a criterion to assess whether the fracture of BMGs is essentially brittle or plastic. If the curvature radius of the crack tip is greater than the critical wavelength of meniscus instability [F. Spaepen, Acta Metall. **23** 615 (1975); A.S. Argon and M. Salama, Mater. Sci. Eng. **23** 219 (1976)], microscale vein patterns and nanoscale dimples appear on crack surfaces. However, in the opposite case, the local quasi-cleavage/separation through local atomic clusters with local softening in the background ahead of the crack tip dominates, producing nanoscale periodic corrugations. At the atomic cluster level, energy dissipation in fracture of BMGs is, therefore, determined by two competing elementary processes, viz. conventional shear transformation zones (STZs) and envisioned tension transformation zones (TTZs) ahead of the crack tip. Finally, the mechanism for the formation of nanoscale periodic corrugation is quantitatively discussed by applying the present energy dissipation mechanism.

1. Introduction

During dynamic fracture of brittle materials, the connection between structure and dissipation has motivated a variety of investigations [1–4]. Complicated morphologies arise as systems shed their excess energy and a detailed understanding of these morphologies is necessary to explain precisely how dissipation occurs. For structurally, relatively-stable brittle materials, such as silicon single crystals, covalent silicate glasses and polymer glasses (PMMA), fracture surfaces exhibit a characteristic pattern sequence known as 'mirror, mist and hackle' [5]: an initially featureless mirror-like fracture surface begins to appear misty and then evolves into a rough hackle region. In such case, the main mechanism for energy dissipation is

*Corresponding author. Email: lhdai@lnm.imech.ac.cn

Philosophical Magazine
ISSN 1478–6435 print/ISSN 1478–6443 online © 2008 Taylor & Francis
http://www.tandf.co.uk/journals
DOI: 10.1080/14786430701864753

the creation of new fracture surface followed by path instability or bifurcation instability [1–4]. As for metallic glasses with unique amorphous structures and mechanical behaviours [6–12], their dynamic crack processes exhibit much more intricate fracture patterns: (i) ubiquitous microscale cell or river-like vein patterns [13–17], (ii) nanoscale dimples and periodic corrugations observed very recently on regions corresponding to featureless mirror zones of silicate glasses or PMMA [18–25], and (iii) even featureless mirror zones at atomic scale [25]. This diversity in patterns indicates that the fundamental principles and mechanisms that underpin the fracture properties of metallic glasses are distinctive, compared with crystalline alloys [26–29]. The fluid meniscus instability or local softening per se, has successfully simulated microscale cell or river-like vein patterns [27, 28] and may be still valid for explaining the formation of these brand-new nanometre-scale patterns [24]. Indeed, recent studies indicate that the local plastic flow (or softening) ahead of the crack tip is truly an essential dissipation process [18, 19, 24, 25]. On the other hand, it is worth pointing out that the local cleavage mechanism is also considered to be proactive in some cases [20]. The question whether fracture of metallic glasses is brittle or plastic, that is the underlying physical origin of fracture, has been discussed extensively but still remains controversial [29–31]. In addition, we noted that recent studies have mainly focused on ideally or less *brittle* bulk metallic glasses (BMGs) [18–25]. Naturally, some important questions arise from these investigations. Is this new-found nanoscale patterning universal for all BMGs, irrespective of whether they are brittle or tough? What are the implications if the answer is affirmative and what is the correlation between energy dissipation and their atomic structures?

This article presents an overview of the fracture patterns of a typical tough $Zr_{41.2}Ti_{13.8}Cu_{10}Ni_{12.5}Be_{22.5}$ (Vit 1) BMG, as a model material, focusing specifically on the fundamentals and mechanism of fracture. Compression, tension and high-velocity plate impact experiments were conducted over a wide range of stain rates from $\sim 10^{-4}$ to $10^{6}\,s^{-1}$. For the first time, we found that this tough Vit 1 can also exhibit fine dimple structures at the 100-nm scale and even sub-100 nm periodic corrugations on dynamic mode I fracture surfaces. An energy dissipation mechanism, accounting for the competition between the two elementary processes, namely shear transformation zone (STZ) and tension transformation zone (TTZ), underlying local softening and quasi-cleavage ahead of the crack tip, respectively, is proposed to unify the four types of fracture patterns mentioned above. Typically, the mechanism for the formation of the nanoscale periodic corrugation is quantitatively discussed in terms of STZs and TTZs by applying the present energy dissipation model.

2. Experimental procedure

$Zr_{41.2}Ti_{13.8}Cu_{10}Ni_{12.5}Be_{22.5}$ BMGs were produced by arc-melting elemental Zr, Ti, Cu, Ni and Be with a purity of 99.9% or better together under a Ti-gettered Ar atmosphere to obtain master ingots. To ensure homogeneity, the master alloy ingots were re-melted several times and subsequently suction-cast into copper

moulds with different dimensions, i.e. 5 mm in diameter and 100 mm in length for the samples used for compressive and high-velocity plate impact tests, and $100 \times 20 \times 2$ mm for tensile test specimens. The amorphous structure of the samples was confirmed by conventional X-ray diffraction (XRD) in a Philip PW 1050 diffractometer using Co Kα radiation. As shown in figure 1, the two sample types for mechanical testing showed only broad diffraction maxima and no peaks of crystalline phases were visible, revealing the glassy structure. Specimens for compression tests were obtained by wire electrical discharge machining the as-cast amorphous rods to achieve a gauge of 5 mm in diameter and 8 mm in length. Quasi-static and dynamic compressive tests were performed on an MTS-810 material testing machine and a split Hopkinson pressure bar (SHPB) at room temperature, respectively. In quasi-static compressive tests, the average strain rate, estimated by the velocity of the load head and the sample length, was fixed at $1.0 \times 10^{-4}\,s^{-1}$. In the SHPB dynamic compressive experiments, whose process are detailed previously [16, 32], the average strain rate was fixed at $1.5 \times 10^{3}\,s^{-1}$ by controlling impact velocity. According to the obtained loading pulses and the standard SHPB principle, the average compressive stress and strain was determined. Tensile specimens were machined into dogbone-like shapes to ensure that the deformation occurred in the middle constraint region with dimension of $3 \times 2 \times 2$ mm. Only quasi-static tensile tests were conducted in the MTS-810 machine at a strain rate of $5.0 \times 10^{-4}\,s^{-1}$. A high-velocity plate impact experiment on a thin Vit 1 disk, 0.3 mm thick with the diameter of 5 mm, was performed using a light gas-gun [33]. After testing, an FEI Sirion high-resolution scanning electron microscope (HRSEM) with spatial resolution of 1.5 nm and an optical microscope (OM) were used to characterize the fracture surfaces of all specimens.

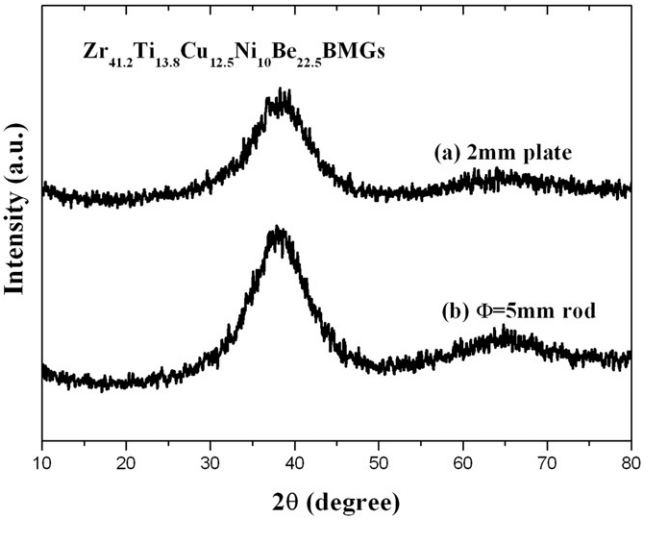

Figure 1. XRD patterns of Vit 1 BMGs for (a) tensile and high-velocity impact tests; (b) compressive tests.

3. Results

3.1. *Quasi-static compressive tests*

Figure 2 presents the fracture behaviour of a Vit 1 sample after compressive testing under a quasi-static strain rate of $1.0 \times 10^{-4}\,s^{-1}$. Figure 2a illustrates the macroscopic side-view of the fracture surface, featuring two distinct regions, I and II.

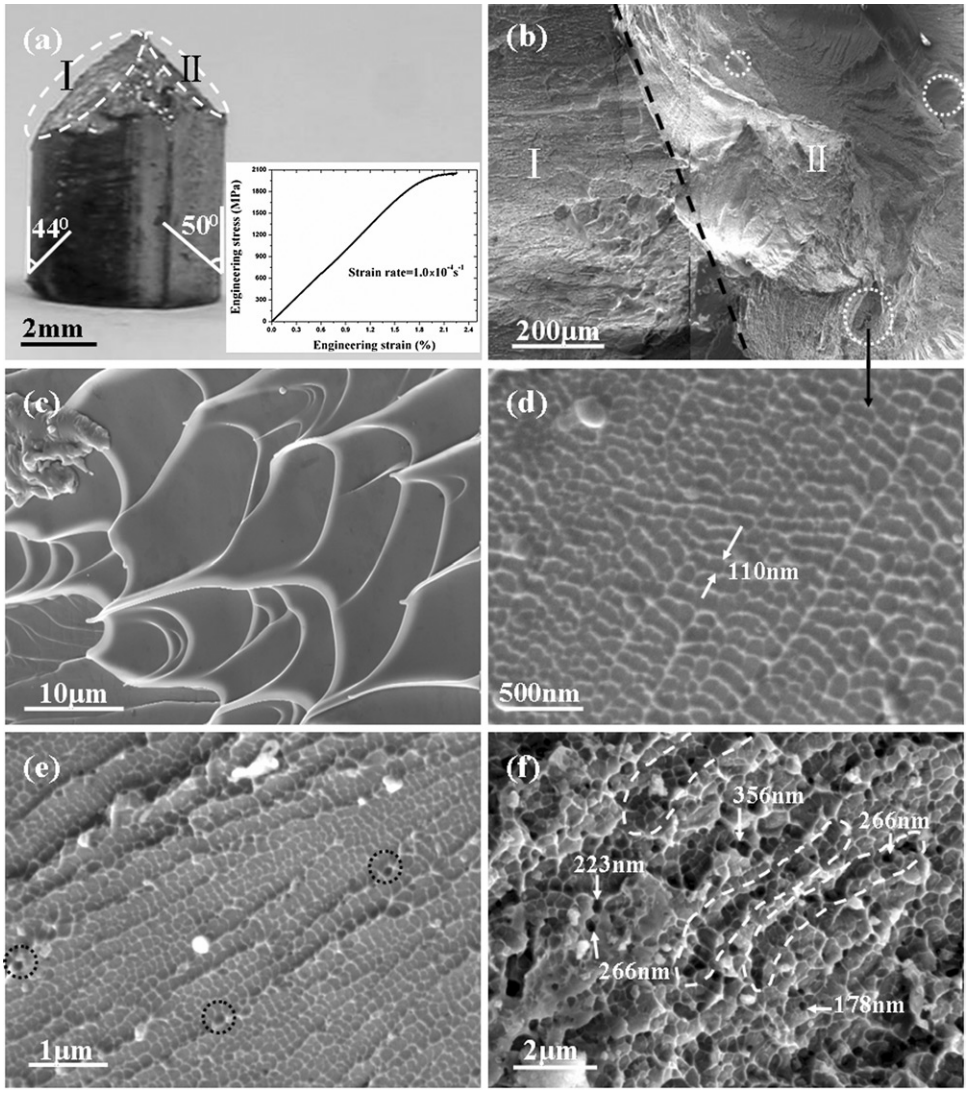

Figure 2. Fracture characteristics of Vit 1 BMG under the quasi-static compression. (a) Macroscopic side-view of the fractured specimen with a sketch of fracture angles; (b) SEM image showing a top-view of the fracture surface; (c) Typical vein patterns on micrometer scale in region I; (d)–(f) Details corresponding to the areas circled in (b).

It was found that the fracture angles corresponding to regions I and II are approximately 44° and 50°, respectively. The average compressive stress–strain curve is shown in the inset to figure 2a, clearly revealing a perfect elastic deformation and a subsequent yielding with an appreciable ductility of ~0.5%. In contrast to the usual ~2% plasticity in other compression [34, 35], there is less plastic flow in the current test, which may be ascribed to the occurrence of region II. Figure 2b shows the top-view of the fracture surface, where the boundary between the two regions is marked by a dashed line. Overall, the fracture surface in region I is relatively flat and displays a typical shear fracture mode, characterized by typical cell-like vein patterns on microscale (figure 2c). However, it can be clearly seen that in region II, there exist a few local mirror or flat zones (circled in figure 2b) randomly distributed on the highly faceted fracture surface. The presence of mirror or flat zones perpendicular to loading direction provides experimental evidence of a dynamic mode I fracture locally [21, 36, 37]. Apparently, the fracture patterns in region II imply that the material experienced a rather complex stress state and obvious bifurcation preceded finally catastrophic failure. Thus, one can speculate that the failure of the Vit 1 rod under quasi-static compression is initially by a slow mode II crack, which is locally transformed to fast mode I at the final stage of the hysterical failure (at the loss of stability in the strained sample at large deformations). This drastic change in crack modes is consistent with the lack of ductility shown by the stress–strain curve. Actually, this instability phenomenon has been widely observed in many other compressive tests on BMGs [21, 38]. Figures 2d–f shows high magnification curves of the circled zone in figure 2b. A large number of dimples at the 100-nm scale are observed, as shown in figure 2d. These dimple structures are strikingly similar to those observed on the fracture surfaces of ideally or less brittle BMGs [18, 19, 22, 24, 25], but have never been seen in tough Vit 1 BMGs. Figure 2e also shows that dimple structures can transform to river patterns. We noted that this transition occurred via a sequence of void formations (dashed circles in figure 2e), indicating that coalescence of free volume plays a key role during the propagation of the crack front [18, 19, 23, 24]. The river pattern is usually regarded as the result of crack-branching at high crack-propagating velocity [1–5, 23, 24]. During transition, both the size and number of damaged voids increase progressively. Finally, these voids form honeycomb structures and the hackle patterns appear as shown in figure 2f. Moreover, some voids larger than ~200 nm are linked (see dashed loops in figure 2f), promoting the increased kinetic energy dissipation of the fast running crack and producing more fracture surfaces. It is important to point out that the transition from dimple to honeycomb structures is ubiquitous in region II. The observations provide powerful evidence for mode I fracture in region II, not least because that void growth and linkage are facilitated by tensile stress [39].

3.2. *Dynamic compressive tests*

Figure 3 shows the typical fracture characteristics of tough Vit 1 BMGs under dynamic compressive loading at a strain rate of $1.5 \times 10^3\,s^{-1}$. The fracture angle is

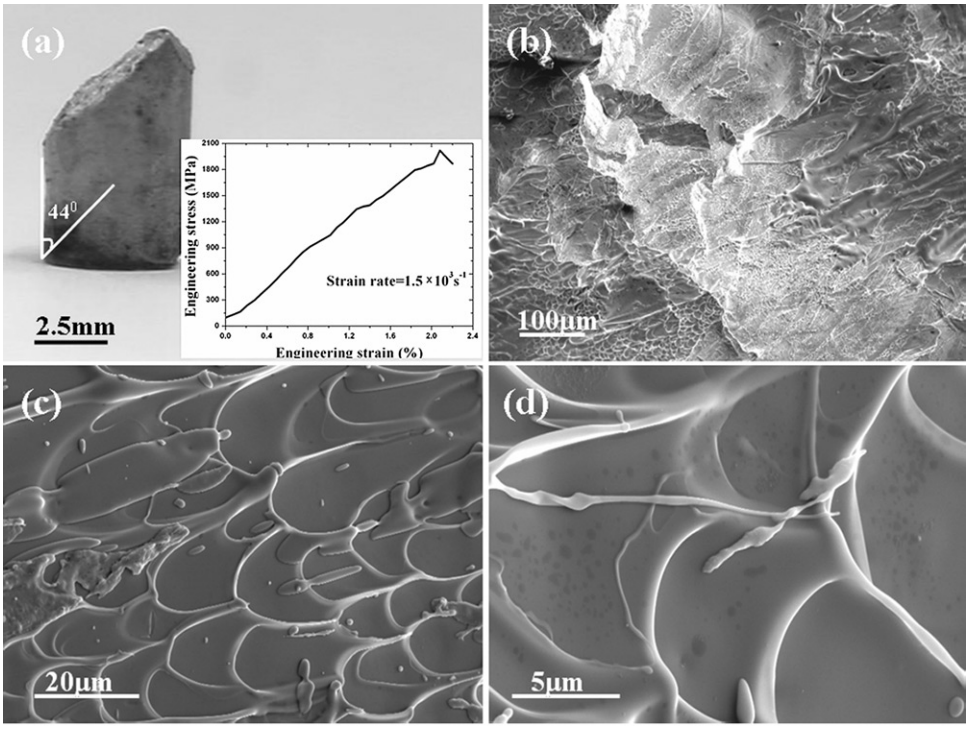

Figure 3. SEM micrographs showing the dynamic compressive fracture feature of Vit 1 BMG. (a) Side-view of the fractured specimen with a sketch of fracture angles. Inset: dynamic compressive stress–strain curve; (b)–(d) Compressive surfaces at different magnification.

equal to 44°, implying that the fracture under dynamic compression also occurs in a shear mode, as seen in figure 3a. The dynamic compressive stress–strain curve is shown in the inset to figure 3a, exhibiting an initial elastic deformation and immediate fractures without any macroscopic plastic flow. Compared to the quasi-static case, several different features of fracture morphology are evident by SEM observations (figures 3b–d). These features are summarized as follows: (1) fracture surface is relatively rough and patterns become more intricate; (2) with the attendant vein patterns, many melted droplets and belts can be clearly observed, which indicates that the temperature rise, induced by the adiabatic shear heating, may exceed the melting temperature of the alloy [16, 40]. Despite these differences, the fracture surface in the dynamic case is also a vein-like structure on a micrometer scale smeared in the direction of shear, as shown in figures 3c and d. These veins on the fractography confirm a pure shear fracture process of the present sample. Detailed observations show that the local mode I crack, similar to that of region II in the quasi-static case, does not occur, which is consistent with zero plastic flow in the dynamic compression case. In addition, the very short duration of dynamic compression may prevent the occurrence of this instability.

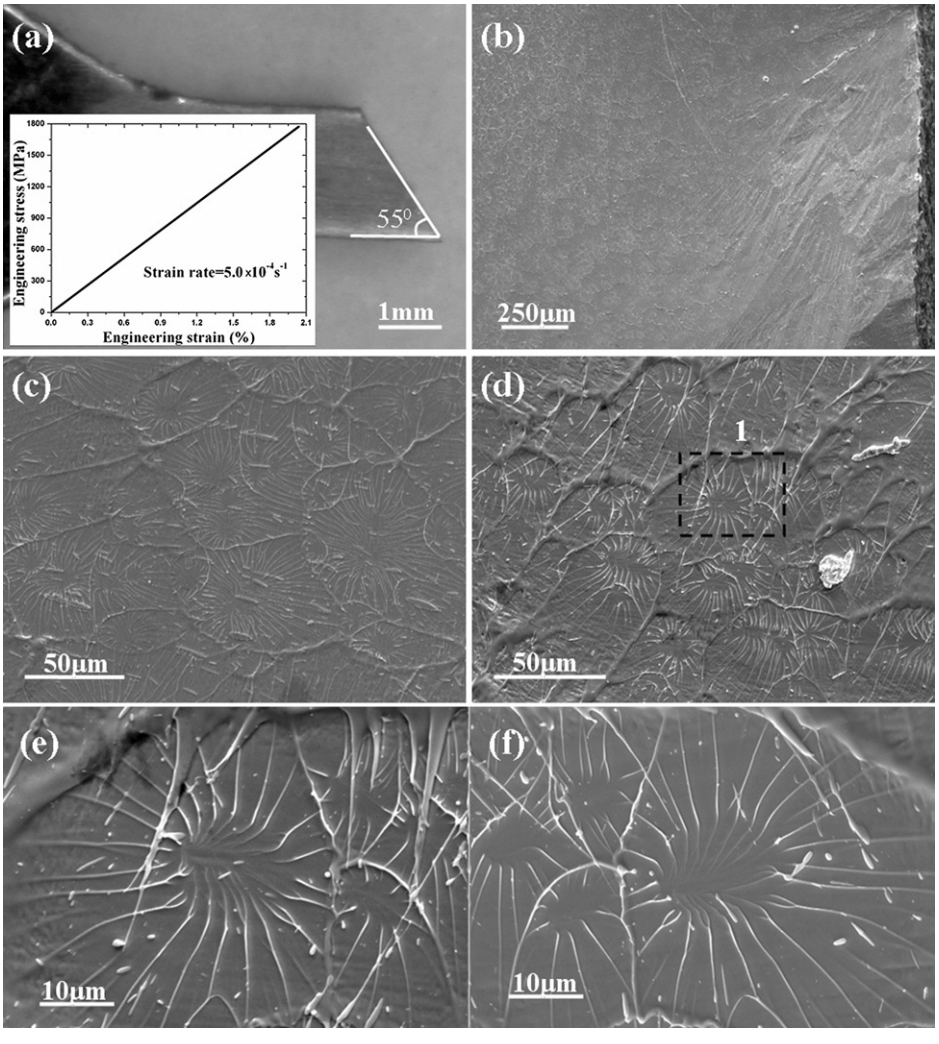

Figure 4. SEM micrographs showing the quasi-static tensile fracture feature of Vit 1 BMG. (a) Side-view of the fractured specimen with a sketch of fracture angles. Inset: tensile stress–strain curve; (b)–(d) Compressive surface at different magnification; (e, f) Comparison of lower and upper surfaces observed by SEM.

3.3. *Quasi-static tensile tests*

The inset in figure 4a gives the tensile stress–strain curve of a Vit 1 specimen deformed at a strain rate of $5.0 \times 10^{-4}\,s^{-1}$. The material displays elastic deformation behaviour only with a strain of ~2.0% and catastrophic fracture without yielding, which differs from the quasi-static compressive tests. The fracture stress is ~1.8 GPa, which is slightly lower than the compressive fracture stress of ~2.0 GPa. OM and SEM observations show that the tensile specimens also fractured in a shear mode, as presented in figure 4. The tensile fracture angle is 55° as marked in figure 4a,

which is significantly different from 45°. The formation and evolution of one major shear band dominates the fracture process. The fracture surface is very smooth (figure 4b) and a vein-like morphology on micrometer scale is visible (figures 4c–f). The result is consistent with previous observations for other metallic glasses under tensile deformation [15, 26, 41, 42].

Further investigations reveal that compared to the compressive fracture planes, the patterning on the tensile fracture surface is distinctive. On the tensile fracture surface, in addition to the vein-like structure, there are many round cores of different diameters, as shown in figures 4c–f. It has been suggested that these round cores correspond to the local sites where failure initiates [15, 36], but are still not well explained. In addition, benefiting from the concision of the tensile fracture surfaces, both surfaces of the fractured Vit 1 BMG observed by SEM were compared. Figure 4e is a high-magnification micrograph of an area, marked '1' in figure 4d, localized in the lower block of the specimen. Figure 4f is the corresponding round core observed on the surface of the upper block. The observations clearly show a peak-to-peak separation during the crack process. Note that, in this case, the separation occurs on a micrometer scale. In fact, Wang *et al*. [24] recently found that this peak-to-peak separation at the crack tip can also take place on a nanometre scale.

3.4. *High-velocity plate impact tests*

Plane shock wave was generated by the high-velocity (up to ~500 m/s) plate impact method using a light gas-gun. Stress analysis on the finite-diameter disk specimen under a plane shock wave indicated that the crack can move in mode I with a strain rate of $\sim 10^6\,s^{-1}$ along a radius from the edge to centre of the disk [33], as marked in figure 5a. It is readily noticed that on a microscale, the fracture surface of the tough Vit 1 BMGs consists in this case of many mirror or flat zones (circled in figure 5a) and some river pattern zones. This pattern is similar to that observed in region II of fracture surface during quasi-static compression, implying that the Vit 1 specimens in both cases fracture in the same mode, i.e. a dynamic mode I fracture. Surprisingly, a periodic corrugation with the average spacing of ~80 nm (figure 5b) clearly appears on the mirror or flat zones. Atomic-force microscopy (AFM) observations on a periodic corrugation are presented in figures 5c–f, in which the fracture surface of Vit 1 is on the x–z plane. The 3D patterning (figure 5c) strikingly shows that the straight corrugations perpendicular to the crack direction (the x direction) is nearly periodic with constant spacing. The section shape of the corrugation is along the red line in figure 5c, i.e. the crack direction exhibits a near sinusoidal curve (figure 5d). The average peak-to-peak distance is ~70 nm. The section shape of the corrugation along the peak, i.e. the cyan line in figure 5c also shows a wavy shape (figure 5e) with an average wavelength of ~40 nm. The presence of characteristic lengths in both directions implies that the local plastic flow (softening) occurs during peak formation [26, 27]. However, it is found that the surface along the valley, i.e. the green line in figure 5c shows a chaotic undulation (figure 5f). This disorder results from intrinsic atomic density fluctuation or free volume stochastically distributed in the material [43, 44].

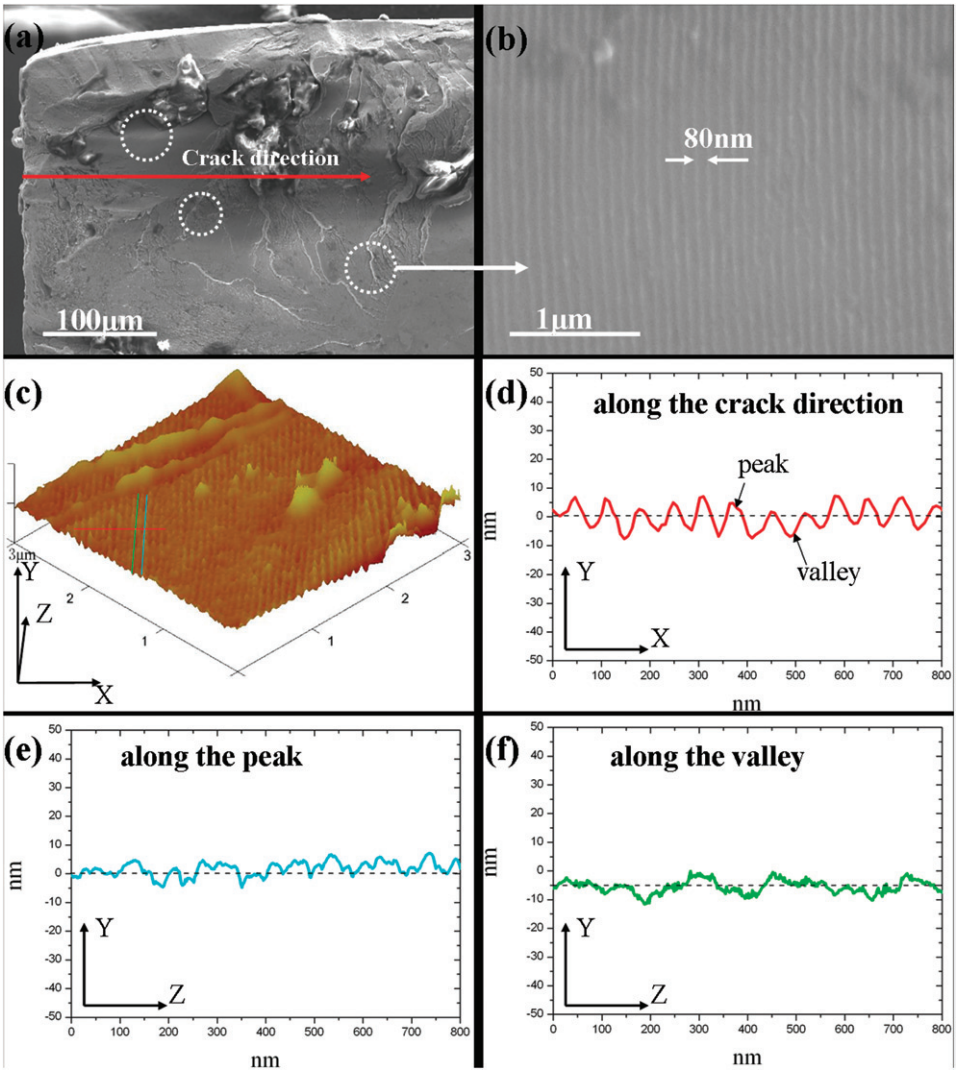

Figure 5. (Colour online) SEM and AFM results showing the fracture feature of Vit 1 BMG under high-velocity impact tests. (a) Dynamic mode I fracture surface near the specimen edge; (b) Details corresponding to areas circled in (a); (c) 3D image of the periodic corrugation on the facture surface, crack propagates along the x-direction; (d) Section shape of the corrugation along the red line in (c), i.e. the crack direction; (e) Section shape of the corrugation along the cyan line in (c), i.e. the peak; (f) Section shape of the corrugation along the green line in (c), i.e. the valley.

Note also that the roughness of the valley is less than that of both the crack direction and the peak. Thus, the local energy dissipation corresponding to the valley formation is no longer local softening and an alternative mechanism should exist (*vide post*). As mentioned above, the nanoscale periodic corrugation is also peak-to-peak [24].

4. Discussion

4.1. *Information extracted from experiments*

The experimental results and observations uncovered some crucial features of BMGs behaviour during failure, as follows:

(1) Normal stress, especially normal tension stress plays a more significant role in the failure of BMGs. Normal tension stress results in a more remarkable deviation (>5°) from the maximum shear stress plane (45°) than in the compression case (<5°). This asymmetry between tension and compression has been widely observed in a variety of metallic glasses [26, 32, 41, 42] and confirmed by molecular dynamics simulation of a model metallic glass [45]. A pure tension stress state without a shear stress component can significantly reduce the characteristic size of fracture patterns (see figures 2d–f and 5b). However, the presence of shear stress leads to well-developed vein patterns (see figures 2c and 4), even at a high strain rate (figure 3).

(2) The fracture process, including loading modes and strain rates (or equivalently crack speeds to a certain extent), can lead to a remarkable change in the scale of fracture patterns from microscale to nanoscale. The scale of fracture patterning, in principle, is indicative of the length scale of local softening ahead of the crack tip [18, 19, 23, 24]. Therefore, the local softening of a given BMG can occur at different length scales during different fracture processes.

(3) Note, in particular, that dynamic mode I crack is prone to restrain local softening ahead of the crack tip or favourable for nanoscale pattern formation. For comparison, all available results for nanoscale periodic corrugations formation of metallic glasses are listed in table 1. It can be seen that mode I fracture should be a necessary condition for the formation of periodic corrugations for a wide variety of metallic glasses from ideally

Table 1. Summary of observations of periodic corrugation formation in metallic glasses.

Metallic glass (composition in at %)	Experimental method	Fracture mode	Corrugation spacing (nm)	Refs.
$Mg_{65}Cu_{25}Tb_{10}$	3-point bending of single-edge notched rod	I	~100	[18, 19]
$Mg_{65}Cu_{20}Ni_5Gd_{10}$	3-point bending of single-edge notched rod	I	~50	[22]
$Mg_{65}Cu_{25}Gd_{10}$	3-point bending of single-edge notched rod	I	≤60	[24, 25]
$Fe_{73.5}Cu_1Nb_3Si_{13.5}B_9$	uniaxial tension of ribbon with a 'seed' crack	I	≤70	[23]
$Fe_{65.5}Cr_4Mo_4Ga_4P_{12}C_5B_{5.5}$	compression loading	either I or II	15–50	[20, 46]
$Ni_{42}Cu_5Ti_{20}Zr_{21.5}Al_8Si_{3.5}$	Compression of rod	I	~60	[21]
$Zr_{41.2}Ti_{13.8}Cu_{10}Ni_{12.5}Be_{22.5}$	Planar shock wave testing of thin disk	dynamic mode I	~80	This paper

or less brittle to tough. Besides, we can take 100 nm as upper-bound estimate of periodic corrugation spacing.

(4) In BMGs, fracture pattern formation on crack surfaces is a peak-to-peak separation process, whose dimensions can be nanoscale. This is very different from the observed features of silicate glasses, in which the peaks on one side of the fracture surface fit the valleys on the corresponding facture surface, consistent with the idea of a completely brittle crack [47].

These features imply that fracture patterns at different length scales may correspond to different energy dissipation mechanisms during fracture of metallic glasses.

4.2. *Energy dissipation mechanism*

As bonding in metallic glasses is primarily metallic in character, strain can be readily accommodated at atomic level through changes in neighbours. Atomic bonds can be broken and reformed at the atomic scale without substantial attention to, for example, the rigidity of bond angles, as in a covalent solid, or the balance of charges, as in an ionic solid [12]. Therefore, although they usually undergo a strong tendency for shear localization [48] and macroscopically brittle crack at room temperature, it is far from clear that metallic glasses are capable of legitimate plastic flow or softening at the microscale or even nanoscale [12, 18]. Intrinsic plastic flow on a nanoscale ensures that fluid meniscus instability always occurs in BMGs. In fact, even in an ideally brittle Mg-based BMG with fracture toughness of 1–2 MPa$\sqrt{\text{m}}$, which approaches the ideal brittle behaviour associated with silicate glasses, the instability criteria is also satisfied [24], not to mention tough BMGs, e.g. Vit 1. However, the development of instability must satisfy the following condition [27, 28]

$$\lambda \geq \lambda_c = 2\pi\sqrt{\frac{\chi}{\mathrm{d}\sigma/\mathrm{d}x}}. \tag{1}$$

where λ is the wavelength of the initial perturbation of the meniscus, λ_c is a critical length, χ is surface energy and $\mathrm{d}\sigma/\mathrm{d}x$ is the negative pressure gradient in the front of the crack tip. This equation indicates that, if the wavelength of the initial perturbation is greater than critical, the initial meniscus instability will grow. By applying Taylor's meniscus instability criterion [49] to the fracture process at the tip of a blunted crack undergoing inelastic deformation, λ_c can be further calculated by [27, 28]:

$$\lambda_c = \frac{\lambda_s}{\sqrt{3}}, \tag{2}$$

where λ_s is the dominant wavelength of the instability that leads immediately to the final pattern size. λ_s is given by [28]:

$$\lambda_s = 12\pi^2 A(n)\chi/\tau_y. \tag{3}$$

where τ_y may be taken as the shear yield strength; constant $A(n)$ is the function of non-linearity exponent n, which ranges from unity (Newtonian viscous) to zero (ideal plastic). Due to the presence of inherent plastic flow in BMGs, the singularities in the linear elasticity solutions, stemming from the sharp slit approximation, simply cannot be reconciled with any realistic local rupture process, while nonlinearity is an essential factor [1]. Thus, to properly understand the actual mechanism of crack propagation, Irwin and Orowan [50–52] postulated a 'fracture process zone', in which any nonlinearity is assumed to be confined to a small, well-defined region immediately surrounding the crack tip. Consequently, the initial perturbation of the meniscus must be confined to the frontal nonlinear process zone; the wavelength of the initial perturbation, λ, is not greater than its characteristic size, viz. radius r_p. However, the quantitative determination of r_p is largely ambiguous, particularly for BMGs whose plastic deformation or nonlinearity is extremely localized to the tens of nanometre scale [53, 54]. Previous studies have demonstrated that the curvature radius of the crack tip or fluid meniscus, R, can more directly measure the length scale of local softening [24, 55]. In other words, R can characterize the scale of fracture patterns [27–29], ultimately determining the fracture toughness of a given metallic glass [12, 56]. Hence, according to the meniscus instability criterion [27, 28], if R is larger than the λ_c of instability, meniscus instability develops, finally leading to typical vein patterns. In this case, energy dissipates mainly by local plastic flow or softening ahead of the crack tip. If the reverse is true, the perturbation will disappear; hence, the front of the crack tip is always stable and maintains a straight line [22, 24], during which BMGs break with some quasi-cleavage features. Thus, the curvature radius of the crack tip is the key parameter dominating energy dissipation mechanisms that underpin the fracture properties of BMGs. In fact, the value of R is affected by crack speed, crack modes and toughness of material [24], which we will clarify later.

In fracture, definitive answers must be sought at the atomic level, as it is the nature of the cohesive bonding between the constituent atoms in solids which ultimately determines resistance to the passage of a crack. For polycrystalline solids, the crack at its tip advances by atomic decohesion in shear or tension [1], corresponding to slip or cleavage crack, respectively. However, for metallic glasses, their elements, having negative enthalpies of mixing, tend to form characteristic local atomic clusters [57]. These clusters correspond to sites of high free volume [58, 59], through which the crack progress more easily [55]. Consequently, we can reasonably assume that the crack tip moves by preferentially breaking local atomic clusters instead of atoms. Usually, a local cluster of atoms undergoes an inelastic shear distortion to dissipate energy, leading to local softening ahead of the crack tip. This shear-dominant flow event is commonly referred to as a 'shear transformation zone' (STZ) (see figure 6a), introduced by Argon [59] and developed by Falk and Langer [60]. There is general consensus that the fundamental unit-process underlying plastic softening must be a STZ that can accommodate shear strain [12]. Vein patterns and dimple structures undeniably form through the continuous operation of STZs ahead of the crack tip. In parallel, a local atomic cluster that is directly broken by tensile stress can be envisioned and similarly defined as a 'tension transformation zone' (TTZ) (see figure 6b). Through TTZs, stored energy is dissipated mainly by

forming new surfaces, finally resulting in local quasi-cleavage. The occurrence of a TTZ must satisfy the following two conditions:

(1) High levels of tensile stress at the crack tip, due to stress singularity, from the remarkable decrease in R must approach the ideal normal fracture stress σ_{th} of the material. Equally, levels of tensile stress at the tip will also decrease with decreasing σ_{th}. In fact, the tensile fracture criterion proposed by Zhang and Eckert [37] indicates that, once σ_{th} is equal or smaller than $\sqrt{2}$ times the critical shear fracture stress, normal cleavage crack will occur [37].
(2) The time scale of crack propagation must be very short and less than that of structural relaxation or plastic flow stemming from the intrinsic dilatation effect [61–63] in metallic glasses. Thus, a time scale of less than 10° s is expected [64], during which the visco-inelastic medium, behaving as a solid, has insufficient time to fully flow [29]. STZs, therefore, are restrained.

BMGs usually fracture in a shear mode, during which STZs are dominant. In the dynamic quasi-cleavage crack process, TTZs are regarded as a transient activation from STZs satisfying the above conditions. Logically, we suppose that the number of atoms participating in the two types of collective atomic motions is roughly equal.

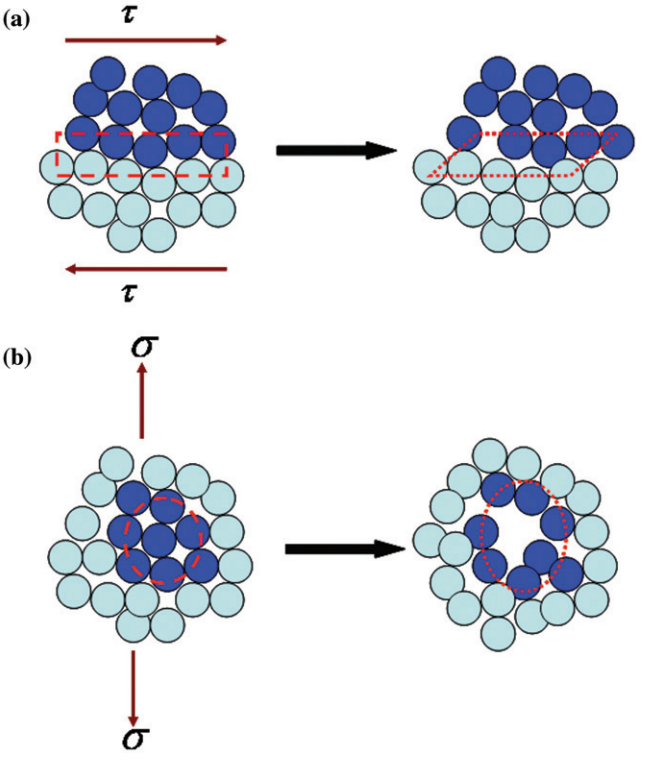

Figure 6. (Colour online) Two-dimensional schematics of collective atomic motion in metallic glasses, including (a) a classical shear transformation zone (STZ), and (b) an envisioned tension transformation zone (TTZ).

It is suggested that an average STZ probably contains 20–30 atoms [12, 65], which depends on the activation energy barrier of STZ [66, 67]. Therefore, the characteristic length size of a STZ or TTZ is estimated at <10 nm [66–68]. Compared to a STZ, which is the elementary process of ductile crack, a TTZ can be considered as the basis of quasi-cleavage, during which tension stress, concentrated in the small process zone ahead of the crack tip, is rapidly alleviated by new surface formation. It is reasonable to believe that STZ and/or TTZ operations on a nanoscale in metallic glasses are responsible for fracture patterning, including conventional vein patterns and new-found nanoscale dimples or periodic corrugations. If $R > \lambda_c$, meniscus instability, as a result of continuing STZs ahead of the crack tip, fully develops. Once $R < \lambda_c$, TTZs control the formation of the fracture pattern, during which some brittle-fracture phenomena, similar to those of silicate glasses for example, emerge on the crack surfaces.

4.3. *Application to fracture processes*

We then applied the proposed energy dissipation mechanism to the fracture processes of tough Vit 1 BMGs presented in section 2. For comparison, a typical ideally brittle $Mg_{65}Cu_{25}Gd_{10}$ BMG is also included. The relevant mechanical properties of these two BMGs are listed in table 2. For BMGs without work-hardening, which approximately behave in an ideally plastic manner, we assume $n \to 0$; hence $A(n) \approx 1.5$ [28]. Using the parameters listed in table 2 and equations (2) and (3), the calculated λ_c for Vit 1 is ~85 nm, which is much smaller than 200 nm for the Mg-based BMG. Thus, the meniscus instability develops more easily in Vit 1 than the Mg-based BMG, which is consistent with experimental observations. The final size λ_s of patterns due to the instability, which assumes no plasticity developing, is 147 and 350 nm for Vit 1 and the Mg-based BMG, respectively. The values roughly compare with the size of the steady-state vein pattern (figures 2d–f) of Vit 1 under mode I crack and dimples (figure 1c in [24] and figure 1b in [25]) observed by Wang *et al.* [24, 25] in the Mg-based BMG. For mode II fracture, the blunting radius R_{II} can be approximately expressed as [55]:

$$R_{II} = \frac{K_{IIC}^2}{(8\tau_y E)} \tag{4}$$

Table 2. Mechanical properties of Young's modulus (E), tension yield strength (σ_y), τ_y, mode I fracture toughness (K_{IC}), mode II fracture toughness (K_{IIC}) and χ for two typical BMGs.

BMGs	E (GPa)	σ_y (GPa)	τ_y (GPa)	K_{IC} (MPa/m$^{1/2}$)	K_{IIC} (MPa/m$^{1/2}$)	χ (J/m^{-2})
Vit 1	~95[a]	~1.8	1.0[b]	15[c]	75[c]	0.83[d]
$Mg_{65}Cu_{25}Gd_{10}$	49.1[a]	0.98[a]	~0.5[e]	2[f]	...	~1[f]

[a]Taken from [69].
[b]Taken from [16].
[c]Taken from [12] and [55].
[d]Taken from [39].
[e]Assuming half of σ_y.
[f]Taken from [18] and [24].

For Vit 1 BMG, the calculated $R_{II} \approx 7\,\mu m$, which coincides well with the actually measured values 4–15 μm (figures 2c, 3c, d and 4c–f). Note that $R_{II} \gg \lambda_s \sim \lambda_c$, indicating that during mode II fracture, the meniscus instability always grows and the size of the local plastic zone is much larger than that of final patterns due to the meniscus instability. In fact, a tensile stress perpendicular to the plane of the layer is only considered during instability analysis, which assumes no plasticity developing [27–29]. It may be deduced that a shear stress can significantly increase the final size of vein patterns because shearing promotes plastic growth [70, 71]. We recognized that during mode II unstable fracture, the meniscus instability is initiated and is then further developed by shearing motion to a more unstable state. This indicates that a shear stress state significantly increases the length scale of local softening from about λ_s to micrometer-scale. Even if no K_{IIC} value of the Mg-based BMG is available as yet, we can speculate that the presence of a shear stress will promote meniscus instability, leading to fracture surface roughening. For mode I fracture, the blunting radius is given by [55]:

$$R_I = \frac{K_{IC}^2}{(4\sigma_y E)} \tag{5}$$

The calculated $R_I \approx 325\,nm$ for Vit 1, which roughly compares with the size of both the steady-state vein pattern (figure 2d–f) and the calculated λ_s. In addition, the relationship of mode I fracture roughness and crack tip open displacement (CTOD) was established as [28]:

$$K_{IC} = \sqrt{(CTOD)\pi\sigma_y E/2.7} \tag{6}$$

where the CTOD is roughly double the blunting radius or the characteristic size of the steady-state corrugation. Based on the observation in figures 2d–f, the $(CTOD)_I \approx 500\,nm$. The calculated K_{IC}, which is $\sim 10 MPa\sqrt{m}$, agrees well with the measured value ($\sim 15 MPa\sqrt{m}$) [12, 55]. The agreement indicates that the fluid meniscus instability controls crack propagation during the whole process of mode I fracture. The above analysis clearly indicates that the formation of both microscale vein patterns and nanoscale dimples is triggered by fluid meniscus instability, during which energy dissipates mainly by local softening or plastic deformation at the crack tip [27, 28]. If there is no shear-stress component, dimple structures are observed, but if a shear stress is present, well-developed vein patterns can emerge. Reverting to the atomic scale, STZs operations ahead of the crack tip play a crucial role on both pattern formations. However, for the Mg-based BMG, the R_1 is calculated to be $\sim 21\,nm$. The R_1 value is much smaller than its λ_c, implying that, during mode I fracture even at quasi-static strain rates, the initial perturbation in Mg-based BMG does not actually develop [24]. This is the reason why nanoscale periodic corrugation can be widely observed in brittle Mg-based BMGs (table 1).

We also noted that strain rates or crack speeds significantly influence R [1], especially in mode I crack. The radius of curvature of the crack tip R decreases rapidly with increasing crack speed V; it becomes zero for a perfectly sharp crack at V equal to 0.5 of the shear wave speed [72]. During dynamic mode II fracture, the shear-stress component enlarges R remarkably, impeding the drop-off in R due to

increasing V. Therefore, the length scales of the local softening do not change noticeably under the two strain rates (figures 2c, 3c and d). However, in mode I fracture, due to slight differences in R_1 and λ_c for Vit 1, increasing V leads to $R_1 < \lambda_c$. Thus, the meniscus instability is restrained in Vit 1 as the brittle Mg-based BMG, leaving straight crack front lines (figure 5b). The question is: what will occur in such a case? More specifically, how does the straight crack front move forward or the excess energy dissipates during the occurrence of the nanoscale periodic corrugations?

We now consider crack growth in the plane strain mode I to quantitatively discuss the formation of nanoscale periodic corrugations, whose two-dimensional schematic representation is illustrated in figure 7.

When a BMG fails at a macroscopic yield stress σ_y, a crack with radius R initiates on the specimen surface, as shown in figure 7a, because the free surface lowers the nucleation energy of the crack. During propagation of the crack, once the condition $R < \lambda_c$ is satisfied, the meniscus instability-induced crack propagation is impeded because the local softening zone ahead the crack tip is so small. At the same time, the stress singularity, arising from R decreasing to nanoscale, results in the

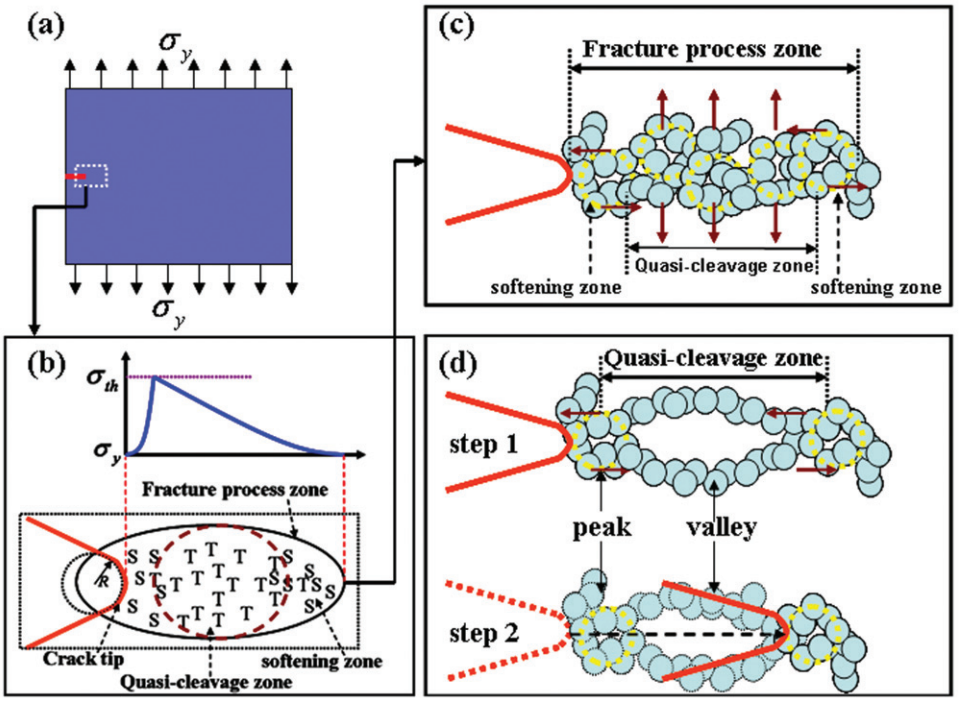

Figure 7. (Colour online) Schematic representation of periodic corrugation formation on facture surfaces in metallic glasses under dynamic mode I crack (a); (b) Illustration of a crack tip with a fracture process zone, during which a local quasi-cleavage zone is present; (c) Amplified view of atom cluster motions ahead of the crack tip; (d) Periodic corrugation forms by the occurrence of local quasi-cleavage neat the tip; coalescence of the local quasi-cleavage zone with the crack yields a longer crack.

tensile stress perpendicular to the crack direction reaching a peak near the crack tip. This stress singularity may be associated with the small sampling volume near the crack tip and the distribution of free volume in glasses [55]. Peak stress must correspond to the theoretical strength σ_{th} of the solid, i.e. the largest possible stress level that the atomic structure can sustain by virtue of intrinsic bond strength [1, 24]. Due to the presence of peak-tension stress, several TTZs ahead the crack tip arise. Thus, we can envisage that a local quasi-cleavage zone comprising several TTZs exists in the pre-formed fracture process zone, as shown in figure 7b where 'S' and 'T' represent STZ and TTZ, respectively. Figure 7c exhibits an amplified view of atom cluster motions ahead of the crack tip. The local quasi-cleavage zone provides a medium through which the stress decays rapidly, matching the high theoretical strength σ_{th} on one side and the low background macroscopic yield strength σ_y on the other. This dramatic decrease in tensile stress should contribute to the fast formation of new surface. As shown in figure 7d, local quasi-cleavage is step 1 in the formation of periodic corrugation. Motivated by Suo *et al*. [73], the dimension (L) of the local quasi-cleavage zone can be approximately estimated by:

$$L = b\left(\frac{\sigma_{\text{th}}}{\sigma_{\text{y}}}\right)^2 \tag{7}$$

where b is the TTZs spacing, which is considered to be of the same order as the characteristic length size of a TTZ itself due to metallic glass's structural similarity to the 'dense random packing of spheres' model [74, 75]. Thus, b is also less than 10 nm at a rough estimate and on a nanometre scale. Assuming the Tresca or von Mises criteria are approximately satisfied, $\sigma_{\text{th}}/\sigma_{\text{y}} \approx \tau_{\text{th}}/\tau_{\text{y}}$, where τ_{th} is the theoretical shear-yield strength close to Frenkel's theoretical limit of a tenth of the shear modulus G [76]. Considering $\tau_{\text{y}} \approx 0.5\sigma_{\text{y}}$ and further using the experimental data presented by Johnson *et al*. [69], we obtain $\tau_{\text{th}}/\tau_{\text{y}} \sim 3.19$. Based on the results of HRR asymptotic solution [77, 78], σ_{th} is calculated as $3 \times \sigma_{\text{y}}$ at $n \to 0$ under one-dimensional simplification [79]. Nanoindentation experiments also reveal a similar ratio of 3.47 [39]. Therefore, reasonably choosing $(\sigma_{\text{th}}/\sigma_{\text{y}})^2 \approx 10$, then the calculated L is (or smaller than) about 100 nm. This value is in a good agreement with the actually measured values of spacing of the periodic corrugations (table 1). The agreement tells us that the local quasi-cleavage mechanism plays a crucial role in the formation of periodic corrugations. In fact, the local quasi-cleavage zone corresponds to the relatively smooth valley part of the periodic corrugation. At the end of step 1, a few STZs operations between the crack surface and the local cleavage zone are activated due to transitory delay of crack propagation speed and the shear-induced dilatation effect [61–63]. Subsequently, the coalescence of the local quasi-cleavage zone with the crack yields a longer crack (step 2 in figure 7d) due to the negative pressure mismatch [27–29]. The coalescence site corresponds to the peak part of the periodic corrugation. At this time, a corrugation period including a peak and a valley forms and the second cycle is set up. One can thus conclude that alternatively activation of TTZs and STZs ahead of the crack tip leads to the arrest (step 1) and propagation (step 2) of a mode I crack, which gives rise to formation of periodic corrugations.

An extreme situation can be predicted. If local softening is ignored ($R \to 0$) due to higher V and/or lower fracture toughness, only TTZs are activated ahead of the crack tip. Then, the crack may propagate with an atomically sharp crack tip, leaving featureless mirror zones [25] before instability. However, an important fact needs to be clarified. In metallic glasses, the shear of randomly close-packed atoms can cause dilatation [61–63]; thus, either process of energy dissipation, i.e. local softening and quasi-cleavage, does not occur alone. In most cases, local softening plays a dominant role in blunting the crack tip where local quasi-cleavage still occurs [24, 28, 29]. However, when local softening is restrained to a nanoscale, local quasi-cleavage dominates fracture patterning, during which local softening is also active, but weaker. Therefore, during the formation of periodic corrugation, the alternatively activation of TTZs and STZs is a gradual transition process. In this sense, fracture of metallic glasses is neither brittleness nor plasticity, or both brittleness and plasticity. Their fracture behaviours are determined by the inherent competition between the two processes of energy dissipation in BMGs. Local softening induces meniscus instability, while local quasi-cleavage fracture is usually followed by path instability and propagation of multiple cracks. The presented energy dissipation mechanism may increase our understanding, at the atomic cluster level, of the Poisson's ratio criterion, suggested by Lewandowski *et al*. [30, 31] as well as parameter α (the ratio of the theoretical shear cleavage strength to the theoretical tension strength) proposed by Zhang, Eckert and co-workers [36, 37], controlling the deformation and failure of BMGs.

5. Conclusions

We attempted to assess whether the fracture of BMGs is essentially brittle or whether some plastic flow or softening accompanies fracture. The criterion proposed that if the size of plastic process zone ahead of the crack tip, which can be characterized by the curvature radius of crack tip, is greater than the critical length of the meniscus instability, a fracture with some softening is possible. If the converse is true, the BMG must break with some or even fully quasi-cleavage features. The fundamental unit process underlying plastic softening must be a local rearrangement of atoms, referred to as 'shear transformation zone' (STZ), that can accommodate shear strain. Thereafter, a collective atomic motion, namely 'tension transformation zone' (TTZ) is envisioned to be the basis of quasi-cleavage, during which tension stress, concentrated in the small process zone, is rapidly mitigated. Energy dissipation in metallic glasses is, therefore, determined by two competing element processes, viz. STZ or TTZ, ahead of the crack tip. If STZs dominate, well-developed vein patterns and dimple structures are clearly observed; conversely, nanoscale periodic corrugations and even mirror zones emerge. The criterion results are in broad qualitative agreement with experiments. It is clear that that alternative activation of TTZs and STZs ahead of the crack tip leads to the arrest and propagation of a mode I crack, which gives rise to formation of periodic corrugations. However, the characteristic spacing of periodic corrugation is determined by local quasi-cleavage cracking. Our study is an important step in understanding the failure mechanisms

of BMGs or other amorphous materials. Furthermore, modification of material compositions and structures in favour of STZs at crack tips will hinder brittle cleavage cracking. This will improve the ductility and reliability of BMGs [80, 81], which is critical for future applications [10].

Acknowledgements

The authors are grateful to Professor B. C. Wei and Dr J. S. Gu for their assistance in material preparation. Financial support from the Natural Science Foundation of China (Grants Nos. 10725211, 10721202) and the Key Project of Chinese Academy of Sciences (Nos.KJCX-SW-L08 and KJCX2-YW-M04) is acknowledged.

References

[1] B. Lawn, *Fracture of Brittle Solids* (Cambridge University Press, Cambridge, 1993).
[2] J. Fineberg, S. Gross, M. Marder, *et al*., Phys. Rev. Lett. **67** 457 (1991).
[3] K. Ravi-Chandar and W.G. Knauss, Int. J. Fract. **26** 65 (1984).
[4] T. Cramer, A. Wanner and P. Gumbsch, Phys. Rev. Lett. **85** 788 (2000).
[5] J.W. Johnson and D.G. Holloway, Phil. Mag. **14** 731 (1966).
[6] A.L. Greer, Science **267** 1947 (1995).
[7] W.L. Johnson, MRS Bull. **24** 42 (1999).
[8] A. Inoue, Acta Mater. **48** 279 (2000).
[9] W.H. Wang, C. Dong and C.H. Shek, Mater. Sci. Eng. R **44** 45 (2004).
[10] M.F. Ashby and A.L. Greer, Scripta Mater. **54** 321 (2006).
[11] J. Eckert, J. Das, S. Pauly, *et al*., J. Mater. Res. **22** 285 (2007).
[12] C.A. Schuh, T.C. Hufnagel and U. Ramamurty, Acta Mater. **55** 4067 (2007).
[13] C.T. Liu, L. Heatherly, D.S. Easton, *et al*., Metall. Mater. Trans. A **29** 1811 (1998).
[14] T. Mukai, T.G. Nieh, Y. Kawamura, *et al*., Scipta Mater. **46** 43 (2002).
[15] Z.F. Zhang, J. Eckert and L. Schultz, Acta Mater. **51** 1167 (2003).
[16] L.F. Liu, L.H. Dai, Y.L. Bai, *et al*., J. Non-Cryst. Solids **351** 3259 (2005).
[17] D.C. Qiao, G.J. Fan, P.K. Liaw, *et al*., Int. J. Fract. **29** 2149 (2007).
[18] X.K. Xi, D.Q. Zhao, M.X. Pan, *et al*., Phys. Rev. Lett. **94** 125510 (2005).
[19] X.K. Xi, D.Q. Zhao, M.X. Pan, *et al*., Appl. Phys. Lett. **89** 181911 (2006).
[20] Z.F. Zhang, F.F. Wu, W. Gao, *et al*., Appl. Phys. Lett. **89** 251917 (2006).
[21] J. Shen, W.Z. Liang and J.F. Sun, Appl. Phys. Lett. **89** 121908 (2006).
[22] D.G. Pan, H.F. Zhang, A.M. Wang, *et al*., J. Alloys Compds. **438** 145 (2007).
[23] G. Wang, Y.T. Wang, Y.H. Liu, *et al*., Appl. Phys. Lett. **89** 121909 (2006).
[24] G. Wang, D.Q. Zhao, H.Y. Bai, *et al*., Phys. Rev. Lett. **98** 235501 (2007).
[25] G. Wang, X.H. Xu, Y.N. Han, *et al*., Phys. Rev. Lett. (2007), submitted.
[26] C.A. Pampillo, J. Mater. Sci. **10** 1194 (1975).
[27] F. Spaepen, Acta Metall. **23** 615 (1975).
[28] A.S. Argon and M. Salama, Mater. Sci. Eng. **23** 219 (1976).
[29] F. Spaepen, *Physics of Defects* (North-Holland, Amsterdam, 1981).
[30] J.J. Lewandowski, W.H. Wang and A.L. Greer, Phil. Mag. Lett. **85** 77 (2005).
[31] J.J. Lewandowski, M. Shazly and A. Shamimi Nouri, Scipta Mater. **54** 337 (2006).

[32] L.F. Liu, L.H. Dai, Y.L. Bai, *et al*., Intermetallics **13** 827 (2005).
[33] J.X. Meng, L.H. Dai and Z. Ling, unpublished data (2008).
[34] H.A. Bruck, T. Christman, A.J. Roskis, *et al*., Scripta Mater. **30** 4296 (1994).
[35] L.F. Liu, L.H. Dai, Y.L. Bai, *et al*., Mater. Chem. Phys. **93** 174 (2005).
[36] Z.F. Zhang, G. He, J. Eckert, *et al*., Phys. Rev. Lett. **91** 045505 (2003).
[37] Z.F. Zhang and J. Eckert, Phys. Rev. Lett. **94** 094301 (2005).
[38] V.Z. Bengus, E.D. Tabachnikova, J. Miškuf, *et al*., J. Mater. Sci. **35** 4449 (2000).
[39] W.J. Wright, Doctoral thesis, Stanford University (2003).
[40] J.J. Lewandowski and A.L. Greer, Nat. Mater. **5** 15 (2006).
[41] J. Megusar, A.S. Argon and N.J. Grant, Mater. Sci. Eng. **38** 63 (1979).
[42] A. Inoue, W. Zhang, T. Zhang, *et al*., Acta Mater. **49** 2645 (2001).
[43] M.H. Cohen and D.J. Turnbull, J. Chem. Phys. **31** 1164 (1959).
[44] A.S. Argon, J. Appl. Phys. **39** 4080 (1968).
[45] A.C. Lund and C.A. Schuh, Acta Mater. **51** 5399 (2003).
[46] M. Stoica, J. Eckert, S. Roth, *et al*., Intermetallics **13** 764 (2005).
[47] J-P. Guin and S.M. Wiederhorn, Phys. Rev. Lett. **92** 215502 (2004).
[48] A.V. Sergueeva, N.A. Mara, J.D. Kuntz, *et al*., Phil. Mag. **85** 2671 (2005).
[49] D.I. Taylor, Proc. R. Soc. (Lond.) A **201** 192 (1950).
[50] G.R. Irwin, *Fracturing of Metals* (American Society of Metals, Cleveland, 1948).
[51] E. Orowan, Rep. Prog Phys. V–XII (1948).
[52] G.R. Irwin, J. Appl. Mech. **24** 361 (1957).
[53] P.E. Donovan and R. Maddin, Acta Metall. **19** 725 (1981).
[54] Y. Zhang and A.L. Greer, Appl. Phys. Lett. **89** 071907 (2006).
[55] K.M. Flores and R.H. Dauskardt, J. Mech. Phys. Solids **54** 2418 (2006).
[56] F.G. Emmetich, J. Appl. Phys. **102** 073504 (2007).
[57] C. Dong, Q. Wang, J.B. Qiang, *et al*., J. Phys. D **40** R273 (2007).
[58] F. Spaepen, Acta Metall. **25** 407 (1977).
[59] A.S. Argon, Acta Metall. **27** 47 (1979).
[60] M.L. Falk and J.S. Langer, Phys. Rev. E **57** 71925 (1998).
[61] J. Li, F. Spaepen and T.C. Hufnagel, Phil. Mag. **82** 2623 (2002).
[62] F. Spaepen, Nat. Mater. **5** 7 (2006).
[63] M.Q. Jiang and L.H. Dai, Phys. Rev. B **76** 054204 (2007).
[64] D. Suh and R.H. Dauskardt, J. Mater. Res. **17** 1254 (2002).
[65] M. Heggen, F. Spaepen and M. Feuerbacher, J. Appl. Phys. **97** 033506 (2005).
[66] S.G. Mayr, Phys. Rev. Lett. **97** 195501 (2001).
[67] M. Zink, K. Samwer, W.L. Johnson, *et al*., Phys. Rev. B **73** 172203 (2006).
[68] J.D. Stevenson, J. Schmalian and P. Wolynes, Nat. Phys. **2** 268 (2006).
[69] W.L. Johnson and K. Samwer, Phys. Rev. Lett. **95** 195501 (2005).
[70] P. Lowhaphandu and J.J. Lewandowski, Scripta Mater. **38** 1811 (1998).
[71] R.D. Conner, A.J. Rosakis, W.L. Johnson, *et al*., Scripta Mater. **37** 1373 (1997).
[72] X.S. Tang and G.C. Sih, Theor. Appl. Fract. Mech. **42** 99 (2004).
[73] Z. Suo, C.F. Shih and A.G. Varias, Acta Metall. Mater. **41** 1551 (1993).
[74] D.J. Bernal, Nature (Lond.) **185** 68 (1960).
[75] X.–P. Tang, U. Geyer, R. Busch, *et al*., Nature (Lond.) **402** 160 (1999).
[76] J.Z. Frenkel, Phys. **37** 572 (1926).
[77] J.W. Hutchinson, J. Mech. Phys. Solids **16** 13 (1968).
[78] J.R. Rice and G.F. Rosengren, J. Mech. Phys. Solids **16** 1 (1968).
[79] J.L. Yu and Z.M. Zheng, Acta Mech. Sinica (in Chinese) **16** 485 (1984).
[80] Y. Zhang, W.H. Wang and A.L. Greer, Nat. Mater. **5** 857 (2006).
[81] Y.H. Liu, G. Wang, R.J. Wang, *et al*., Science **315** 1385 (2007).